

Resistivity of V_2O_3 thin films deposited on a -plane (110) and c -plane (001) sapphire by pulsed laser deposition

B. S. Allimi,¹ S. P. Alpay,^{1,a)} C. K. Xie,² B. O. Wells,² J. I. Budnick,² and D. M. Pease²

¹Materials Science and Engineering Program, Chemical, Materials, and Biomolecular Engineering and Institute of Materials Science, University of Connecticut, Storrs, Connecticut 06279, USA

²Department of Physics and Institute of Materials Science, University of Connecticut, Storrs, Connecticut 06279, USA

(Received 20 March 2008; accepted 16 April 2008; published online 19 May 2008)

Thin films of V_2O_3 with thickness of 215 nm were grown on a - and c -plane sapphire by pulsed laser deposition with (001) V_2O_3 || (001) Al_2O_3 and (110) V_2O_3 || (110) Al_2O_3 epitaxy. The effects of the growth direction on the electrical resistivity of the films were examined. Films on c -plane sapphire displayed a metal-to-insulator transition at $T=180$ K compared to $T=160$ K in single-crystal V_2O_3 . The films on a -plane sapphire, however, showed an insulator-to-insulator transition at $T=186$ K. The variation in the phase transformation characteristics and the resistivity can be attributed to different levels of strain and commensurate changes in the film morphology. © 2008 American Institute of Physics. [DOI: 10.1063/1.2921787]

Vanadium sesquioxide (V_2O_3) typifies material systems exhibiting a metal-to-insulator transition (MIT) as a function of temperature, pressure, and doping concentration.¹ At a transition temperature of about 160 K at an ambient pressure of 1 atm, V_2O_3 transforms from a rhombohedral paramagnetic metallic (PM) to a monoclinic antiferromagnetic insulator (AFI) phase upon cooling, with a jump in the resistivity of about seven orders of magnitude.² A broad second-order transition also occurs around 500 K from the metallic to a semiconducting state. When doped with transition metals such as Cr or Ti, V_2O_3 undergoes additional transitions where the metallic phase can be stabilized with Ti doping and the insulating phase with Cr doping.¹ Due to these transitions, there is a significant interest in V_2O_3 , both in terms of applied and basic research.³⁻⁷ This interest is not only to explore the full potential of this material for technological applications but also to serve as a model for understanding the physics of the MIT itself.

In order to gain more understanding of this material and to explore its full potential for device applications such as thermal sensors, current limiters, positive temperature coefficient thermistors, and optical switches,⁸⁻¹¹ various methods have been devised to synthesize high quality V_2O_3 thin films. Deposition of thin films of this material poses significant challenges because the range of processing parameters for stoichiometric V_2O_3 is relatively small due to the existence of many different oxidation states of vanadium.^{12,13} We have previously shown that it is possible to synthesize high-quality epitaxial V_2O_3 films on sapphire (Al_2O_3) substrates via pulsed laser deposition (PLD) using a powder-pressed pure V_2O_3 target in an evacuated deposition chamber.¹⁴ In this letter, we study the resistivity as a function of temperature of 215 nm thick V_2O_3 films deposited using this methodology on a -plane (110) and c -plane (001) sapphire substrates and compare our findings to the experimental phase diagram of McWhan *et al.*¹⁵

The choice of the different planes of the Al_2O_3 substrate is to examine the effect of the growth orientation on the

films. Figure 1(a) shows the corundum structure¹⁶ of V_2O_3 (which has the same structure as the Al_2O_3 substrate). Figures 1(b) and 1(c) show the epitaxial relation of the different planes (with projection of the atoms on the growth planes) on sapphire substrates (110) V_2O_3 || (110) Al_2O_3 and (001) V_2O_3 || (001) Al_2O_3 . The a -plane (110) has both a and c axes in the plane of growth while the c -plane (001) has only the a axis in the plane with the c axis perpendicular to the plane.

The structural, crystallographic, and surface properties of the films were examined by x-ray diffraction (XRD) and atomic force microscopy (AFM). XRD verified that the films are highly oriented [Fig. 2(a)]. The chemical analysis of the films was carried out via x-ray photoelectron spectroscopy (XPS) and confirmed that both films were indeed V_2O_3 . We determined the thickness of the film by imaging the cross

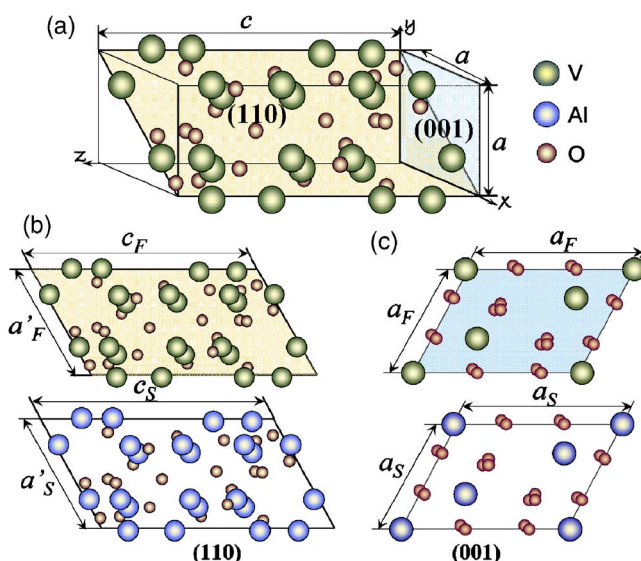


FIG. 1. (Color online) (a) The corundum structure of V_2O_3 and Al_2O_3 showing a - and c -planes. (b) Epitaxy of a -plane V_2O_3 on Al_2O_3 : (110) V_2O_3 || (110) Al_2O_3 . (c) Epitaxy of c -plane V_2O_3 on Al_2O_3 : (001) V_2O_3 || (001) Al_2O_3 . a_F and c_F denote the lattice parameters of the V_2O_3 film while a_S and c_S are lattice parameters of sapphire: $a'_F = a_F\sqrt{3}$ and $a'_S = a_S\sqrt{3}$.

^{a)} Author to whom correspondence should be addressed. Electronic mail: p.alpay@ims.uconn.edu.

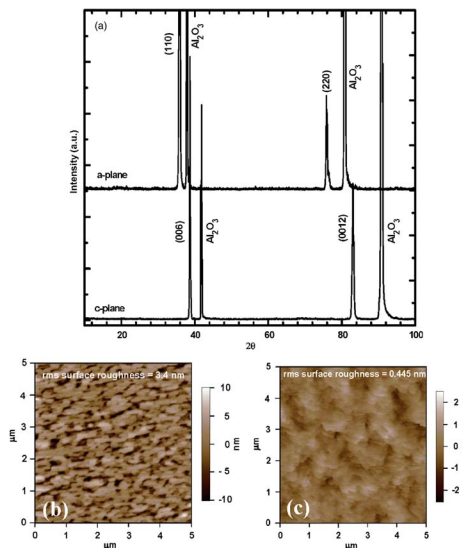


FIG. 2. (Color online) (a) Room temperature XRD patterns of V_2O_3 films on *a*- and *c*-plane sapphire and AFM images of V_2O_3 films on (b) *a*-plane sapphire (c) *c*-plane sapphire substrates.

section of the samples by using field-emission scanning electron microscopy. Experimental details and results were presented in a previous report.¹⁴ Figure 2(a) shows the XRD θ - 2θ diffraction patterns of the films on *a*- and *c*-plane sapphire substrates. We determined the lattice parameters of the films from the combination of the θ - 2θ scan and the result obtained from general area detector diffraction system (GADDS) four-circle diffractometer using the substrate as the reference. The *a* and *c* lattice parameters of the film on *a*-plane sapphire substrate are 0.5014 and 1.3847 nm, respectively, while those on *c*-plane sapphire are 0.4943 and 1.3990 nm, respectively. The results from GADDS four-circle diffractometer also confirmed that both films epitaxially grow on sapphire substrates.

For pseudomorphic V_2O_3 films on *c*-plane sapphire, with only *a*-axis in the plane of growth as shown in Fig. 1(c), the strain components are given by $\varepsilon_1 = \varepsilon_2 = (a_S - a_F)/a_S = -4.1\%$ (isotropic biaxial in-plane strain) and $\varepsilon_3 = -2\varepsilon_1 C_{13}/C_{33} = 3.6\%$. On the other hand, on *a*-plane sapphire with the *a* and *c* axes in the plane of growth as shown in Fig. 1(b), the pseudomorphic strains are given by $\varepsilon_1 = (a_S - a_F)/a_F = -4.1\%$, $\varepsilon_2 = (c_S - c_F)/c_S = -7.8\%$, and $\varepsilon_3 = -C_{13}(\varepsilon_1 + \varepsilon_2)/C_{33} = 5.1\%$, resulting in an anisotropic biaxial in-plane strain. Here, C_{ij} are the strain tensor and the elastic moduli¹⁷ of bulk V_2O_3 in the contracted notation, a_S and c_S are the lattice parameters of the sapphire substrate, and a_F and c_F are the lattice parameters of unconstrained bulk V_2O_3 . From the measured values of *a* and *c* lattice parameters of the films obtained from XRD data on both *a*- and *c*-plane sapphire, we calculated the strain states of the films by comparing measured lattice parameters of the films with that of the bulk. The results indicate that $\varepsilon_1 = \varepsilon_2 = -0.22\%$ and $\varepsilon_3 = -0.13\%$ in the film on *c*-plane sapphire where ε_1 and ε_2 are the strain components along [100] and [010] axes, respectively. In the film on *a*-plane sapphire, $\varepsilon_1 = 1.20\%$, $\varepsilon_2 = -1.15\%$, and $\varepsilon_3 = 1.20\%$. When compared to the theoretical results for pseudomorphic films, we observe that both films have been partially relaxed in plane with varying degrees. AFM results [Figs. 2(b) and 2(c)] show that the surface of the film on *c*-plane sapphire is very smooth (surface roughness of

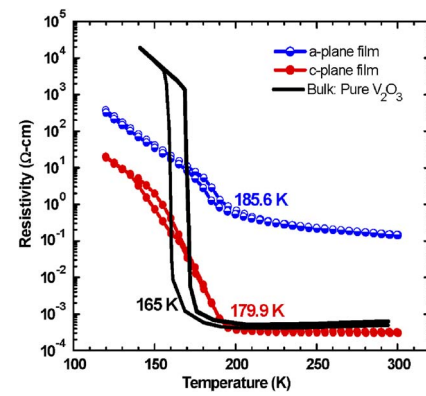


FIG. 3. (Color online) Temperature dependence of resistivity of V_2O_3 thin films deposited on *a*- and *c*-plane sapphire. Resistivity of single crystal V_2O_3 reproduced from Ref. 7 is included for comparison. Transition temperatures of the samples are indicated on the plot.

0.445 nm) compared to the film on *a*-plane sapphire (surface roughness of 3.4 nm). The observed difference in surface roughness in these films can be attributed to the difference in growth modes and commensurate variations in the microstructure of the films due to the different levels of strain.

The electrical resistance measurements as a function of temperature ranging from 110 to 300 K were performed using a Displex system equipped with a Lakeshore temperature controller software package. The Van de Pauw method and standard four-point probe were used to measure the in-plane transport properties of the V_2O_3 films on *c*-plane and *a*-plane sapphire substrates. The *a*-plane (110) substrate was cut into a bar shape such that the *c* axis was the longer side and the *a* axis was the shorter side of the bar. This was done to ensure that the *c*-axis was clearly differentiated from the *a*-axis so that we can account for the anisotropy effects in resistivity measurements.

Figure 3 shows the temperature dependence of resistivity of V_2O_3 thin films on *a*-plane (110) and *c*-plane (001) sapphire. The film on *c*-plane sapphire shows the expected MIT at a temperature of about 180 K (determined by taking the maximum in the derivative of the resistivity plot), although the stability of the metallic phase was reduced by 20 K. The transition is broadened from 140 to 195 K compared to what is observed in single crystal V_2O_3 (also shown in Fig. 3). This behavior has been reported in other V_2O_3 films as well.¹⁸ Films on *c*-plane sapphire substrate with smaller total strain of $\sim 0.22\%$ appear to relax much better as the films are cooled down from the deposition temperature of 1023 K and exhibit the expected MIT, although with a 34 K shift in the transition temperature. For the films on *a*-plane sapphire, we observe a markedly different behavior. There is a transition from one form of insulator to another form (insulator-to-insulator transition) at a temperature of about 186 K. Previous work on the role of crystalline anisotropy on the resistivity of single crystal V_2O_3 showed that the resistivity along the *a* axis and the *c* axis at 273 K are 6.3×10^{-4} and $5.6 \times 10^{-4} \Omega \text{ cm}$,¹⁹ respectively; a difference of only 11%. The significant differences in the electrical properties of our films compared to single crystal values cannot be explained by the variation in the anisotropy of the resistivity. The resistivity of films on *a*-plane sapphire at room temperature (298 K) is $\sim 1.45 \times 10^{-1} \Omega \text{ cm}$ while that on *c*-plane sapphire is $\sim 3.18 \times 10^{-4} \Omega \text{ cm}$.

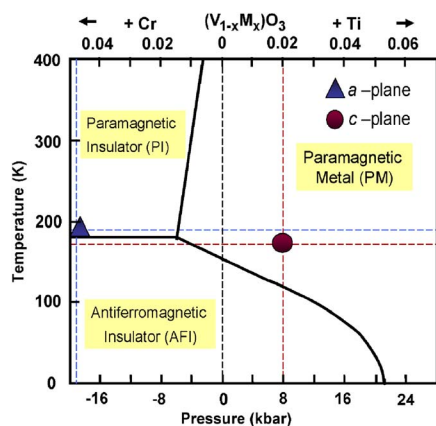


FIG. 4. (Color online) Phase stability regions of PM, PI, and AFI phases in V_2O_3 at room temperature as a function of pressure and doping content (with Cr or Ti), reproduced after Ref. 15. The solid triangle and circle show the possible positions of our V_2O_3 films on *a*- and *c*-plane sapphire, respectively.

We note that there are multiple microstructural factors besides crystalline anisotropy that may have a more profound influence on the electrical properties. The evolution of defect microstructures on epitaxial films is a direct response to the internal stresses that arise due to the lattice and thermal expansion mismatch. In addition to Clausius–Clayperon type thermodynamic effects that alter the phase transition characteristics due to the misfit strain, the resultant film morphology is directly related to the stress relaxation mechanisms and modes of film growth. For example, epitaxial stresses can be relaxed with a varying degree that depends on the film thickness via the formation of misfit dislocations at the deposition temperature. Furthermore, depending on the internal stresses, film deposition may proceed via layer-by-layer growth or by the formation and coalescence of islands.²⁰ The latter growth mode results in the formation of low-angle boundaries, which in turn would alter electrical conductivity.

Films on *a*-plane sapphire, with a significant amount of unrelaxed strain (about 300% higher than that of the film on *c*-plane sapphire substrate) exhibited three orders of magnitude higher resistivity in the 200–300 K range and there is a suppression of the MIT. Similar behavior has been reported in films grown by varying oxygen partial pressure during deposition.⁵ Furthermore, the insulating state can be stabilized via Cr doping in single crystal V_2O_3 .¹⁵ In their investigation of the effects of hydrostatic pressure and doping composition on V_2O_3 , McWhan *et al.* found that Cr doping has an equivalent negative pressure effect on V_2O_3 .^{15,21} Figure 4 shows a schematic reproduction of the phase stability regions of PM, paramagnetic insulating (PI), and AFI phases in V_2O_3 at room temperature as a function of pressure and doping content (with Cr or Ti).¹⁵ One possible way of relating V_2O_3 films under biaxial strain to the phase diagram¹⁵ is by calculating the unit cell volume of the films and comparing it to that of the single crystal under hydrostatic pressure. The isothermal bulk modulus (or the inverse compressibility) is given by $K_T = -V dP/dV$ where V and P are the unit cell volume (0.2977 nm^3 for V_2O_3) and the applied hydrostatic pressure, respectively. Thus, using $K_T = 1.75 \text{ Mbar}$ for V_2O_3 ,²² the pressure axis on the McWhan *et al.* phase diagram can be “converted” to the unit cell volume (4 kbar corresponding to 0.00068 nm^3 in Fig. 4). Using the mea-

sured transition temperatures and calculated unit cell volumes of our films on *a*-plane and *c*-plane sapphire, we have marked on this phase diagram their presumed respective locations with change in unit cell volume associated with V_2O_3 film on *c*-plane and *a*-plane sapphire corresponding to pressures of about 8 and -20 kbar, respectively. The calculated unit cell volumes of the film on *a*-plane— 0.301 nm^3 increased by 1.26% compared to the uncompressed bulk, indicating a negative pressure effect while that of the film on *c*-plane— 0.26 nm^3 is reduced by 0.57%, indicating a positive pressure effect. The film under compression shows metallic behavior as already observed in single crystals¹⁵ where compression tends to decrease atomic distances. This shows a close agreement of our results with the experimental phase diagram.¹⁵ The film on *a*-plane sapphire at room temperature is in the PI stability region and transforms to an AFI state as it is cooled below the transition temperature while the film on *c*-plane is PM at room temperature and transforms to an AFI state when cooled below the transition temperature. Thus, we have shown that the qualitative behavior of strained films of V_2O_3 can be mapped onto the doping-temperature or pressure-temperature phase diagrams of bulk V_2O_3 . However, a quantitative understanding requires explicitly considering the role of biaxial strain in thin films as compared to the hydrostatic pressure that was investigated in bulk samples.

B.A. and S.P.A. gratefully acknowledge the support of the U.S. Army Research Office through Grant No. W911NF-05-1-0528. C.K.X. and B.O.W. gratefully acknowledge the support of the National Science Foundation through Grant No. DMR-0239667.

¹D. B. McWhan and J. P. Remeika, *Phys. Rev. B* **2**, 3734 (1970).

²P. D. Dernier and M. Marezio, *Phys. Rev. B* **2**, 3771 (1970).

³J. H. Park, L. H. Tjeng, A. Tanaka, J. W. Allen, C. T. Chen, P. Metcalf, J. M. Honig, F. M. F. de Groot, and G. A. Sawatzky, *Phys. Rev. B* **61**, 11506 (2000).

⁴B. Sass, C. Tusche, W. Felsch, N. Quaas, A. Weismann, and M. Wenderoth, *J. Phys.: Condens. Matter* **16**, 77 (2004).

⁵H. Schuler, S. Klimm, G. Weissmann, C. Renner, and S. Horn, *Thin Solid Films* **299**, 119 (1997).

⁶I. Yamaguchi, T. Manabe, T. Kumagai, W. Kondo, and S. Mizuta, *Thin Solid Films* **366**, 294 (2000).

⁷S. Yonezawa, Y. Muraoka, Y. Ueda, and Z. Hiroi, *Solid State Commun.* **129**, 245 (2004).

⁸E. Andrich, *Philips Tech. Rev.* **30**, 170 (1969).

⁹D. M. Moffatt, J. P. Runt, A. Halliyal, and R. E. Newnham, *J. Mater. Sci.* **24**, 609 (1989).

¹⁰D. P. Partlow, S. R. Gurkovich, K. C. Radford, and L. J. Denes, *J. Appl. Phys.* **70**, 443 (1991).

¹¹R. S. Perkins, A. Ruegg, M. Fischer, P. Streit, and A. Menth, *IEEE Trans. Compon., Hybrids, Manuf. Technol.* **5**, 225 (1982).

¹²R. G. Mani and S. Ramanathan, *Appl. Phys. Lett.* **91**, 062104 (2007).

¹³G. J. Hyland, *J. Phys. C* **1**, 189 (1968).

¹⁴B. S. Allimi, S. P. Alpay, D. Goberman, T. Huang, J. I. Budnick, D. M. Pease, and A. I. Frenkel, *J. Mater. Res.* **22**, 2825 (2007).

¹⁵D. B. McWhan, J. P. Remeika, T. M. Rice, W. F. Brinkman, J. P. Maita, and A. Menth, *Phys. Rev. Lett.* **27**, 941 (1971).

¹⁶J. L. C. Daams, P. Villars, and J. H. N. Van Vucht, *Atlas of Crystal Structure Types for Intermetallic Phases* (ASM, Materials Park, OH, 1991), Vol. 4, p. 6033.

¹⁷P. D. Dernier and M. Marezio, *Phys. Rev. B* **2**, 3771 (1970).

¹⁸K. D. Rogers, J. A. Coath, and M. C. Lovell, *J. Appl. Phys.* **70**, 1412 (1991).

¹⁹J. Feinleib and W. Paul, *Phys. Rev.* **155**, 841 (1967).

²⁰M. J. Stowell, in *Epitaxial Growth*, edited by J. W. Matthews (Academic, New York, 1975), pp. 437 and 559.

²¹W. F. Brinkman and T. M. Rice, *Phys. Rev. B* **7**, 1508 (1973).

²²Y. Sato and S. Akimoto, *J. Appl. Phys.* **50**, 5285 (1979).